Available online at www.sciencedirect.com
ScienceDirect
International Journal of Thermal Sciences 47 (2008) 136–146
International Journal of Thermal Sciences
www.elsevier.com/locate/ijts

On the use of temperature-dependent physical properties in thermomechanical calculations for solid and hollow cylinders

Hakan Argeso [a], Ahmet N. Eraslan [b,*]

[a] *Department of Mechanical Engineering, Başkent University, Ankara 06530, Turkey*
[b] *Department of Engineering Sciences, Middle East Technical University, Ankara 06531, Turkey*

Received 14 April 2006; received in revised form 2 December 2006; accepted 28 January 2007
Available online 27 March 2007

Abstract

The use of temperature-dependent physical properties in estimating the thermoelastic response of cylinders and tubes is assessed. A computational model in cylindrical polar coordinates is constructed for this purpose. The model incorporates experimental data to describe the temperature dependency of the modulus of elasticity E, the Poisson's ratio ν, the yield strength σ_0, the coefficient of thermal expansion α, and the thermal conductivity k of steel. Various numerical examples, including plane strain and generalized plane strain problems, are handled. The predictions are compared to those that assume: (1) constant Poisson's ratio ν, (2) constant ν and linear variations for E, σ_0, α, and k, (3) constant E, α, k, and ν, and variable yield strength σ_0, (4) constant properties for all. It is shown that, for reliable solutions to thermoelastic problems, the variations of E, σ_0, α, and k with temperature must be taken into account. The inclusion of temperature vs. Poisson's ratio data into the model, though, is not of vital importance.

Keywords: Stress analysis; Thermoelasticity; Temperature-dependent properties; Von Mises' criterion; Shooting method

1. Introduction

It is a well-known fact that the physical properties of engineering materials vary considerably with temperature. Since, in general, the modulus of elasticity E sharply decreases with temperature [1], the strength of the material to elastically resist thermal loads decreases. As a result, plastic deformation takes place under much lower thermal loads than those predicted by solutions with constant physical properties [2–4]. Also, the region deformed plastically propagates more rapidly than constant physical property data because the yield strength σ_0 is very sensitive to temperature changes as well [3,4]. Fully plastic stress states are reached at much lower thermal loads and different modes of plasticization may take place [4]. The temperature dependency of other material properties, i.e. the coefficient of thermal expansion α, the thermal conductivity k, and the Poisson ratio ν, also affect the thermomechanical behavior of the material, but not as much as E and σ_0 [5,6]. Hence, if more dependable solutions to thermal stress problems are needed, the temperature dependency of material properties should be taken into account. However, this requires additional modelling, experimentation and computational efforts. In this sense, the work of Noda [6] is important as it describes the derivation of thermoelastic equations for temperature-dependent properties, and outlines the fundamental work done in this regard until 1986. Governing equations for some basic structures like spherical shells, cylinders, tubes, and thin plates are presented. Also, representative results of temperature-dependent computations in comparison to constant properties are depicted.

Recently, numerous investigations pertaining to the thermally induced elastic and partially plastic deformations of basic structures such as disks, cylinders, and tubes have been carried out considering temperature-dependent properties. Details of these investigations may be found in research articles authored by Eraslan and Kartal [3], by Eraslan and Argeso [4], by Noda [7], by Araki et al. [8], by Eraslan and Orcan [9,10], by Eraslan and Kartal [11], by Eraslan and Argeso [12,13], and in the references cited therein. The differences between con-

* Corresponding author.
E-mail address: aeraslan@metu.edu.tr (A.N. Eraslan).

1290-0729/$ – see front matter
doi:10.1016/j.ijthermalsci.2007.01.029

stant and variable physical property calculations can be evaluated by examining the results of some of these publications.

In the series of investigations [3,4,9–13], the authors performed the formulation in terms of E and ν rather than in terms of the Lame's constants λ and μ [2], and used nonlinear fits to experimental data in order to describe the temperature dependency of E, σ_0, α, and k of steel. However, in all these theoretical studies one of the most important parameters of elasticity, the Poisson ratio ν, was assumed to be independent of temperature. This was partly because of the lack of reliable experimental data, and partly because the modulus of elasticity/shear modulus ratio, i.e. E/G ratio, based on the well-known relation $E/G = 2(1+\nu)$, was thought to remain almost constant at elevated temperatures. On the other hand, a parametric analysis carried out by Eraslan et al. [14] investigated the effect of four parameters k, α, E and ν on the elastic limit heat load in thermally induced deformations of two-layer tubes. In this analysis, elastic limit heat loads were calculated by changing one of these parameters (in the range $\pm 5\%$) at a time, and keeping the others constant at their formal values. It was observed that the elastic limit heat load is affected notably by the change in Poisson's ratio. Hence, there appears a need to assess the effect of the temperature dependency of Poisson's ratio in thermal stress calculations. The purpose of the present study is to bring closure to earlier investigations of the authors by constructing a thermoelastic model which includes a realistic temperature vs. Poisson's ratio data in addition to temperature dependent E, σ_0, α, k. For this purpose, the classical heat generating cylinder and tube problems including axially constrained as well as unconstrained ends are considered, and extended to include the temperature-dependent Poisson's ratio. Although these problems have been treated in the past, they are thought to offer good stands for evaluation. More sophisticated problems, though, may not properly serve the same purpose.

The material properties of high-strength low-alloy steel are taken into consideration. To describe the variation of ν with temperature T for this steel, the data given in *Material Property Database* [1] are used and fitted simply into a second-order polynomial in the range $[0 \leqslant T \leqslant 400\,^{\circ}\mathrm{C}]$:

$$\begin{aligned}\nu &= \nu_0\left(1+\nu_1 T+\nu_2 T^2\right)\\ &= \nu_0\left(1+2.5\times 10^{-4}T-2.5\times 10^{-7}T^2\right)\end{aligned} \tag{1}$$

with $\nu_0 = 0.3$. Similar quadratic forms are fitted to thermal conductivity k and thermal expansion coefficient α as well [3,4]. These are

$$\begin{aligned}k &= k_0\left(1+k_1 T+k_2 T^2\right)\\ &= k_0\left(1-4.0\times 10^{-4}T-2.2222\times 10^{-7}T^2\right)\end{aligned} \tag{2}$$

$$\begin{aligned}\alpha &= \alpha_0\left(1+\alpha_1 T+\alpha_2 T^2\right)\\ &= \alpha_0\left(1+2.5641\times 10^{-4}T+2.1368\times 10^{-7}T^2\right)\end{aligned} \tag{3}$$

where $k_0 = 45$ [W/m °C^2], and $\alpha_0 = 11.7\times 10^{-6}$ [1/°C]. Finally, the variation of Young's modulus E and yield limit σ_0 with temperature T for high-strength low-alloy steel can be represented according to the following empirical relations [9,10]:

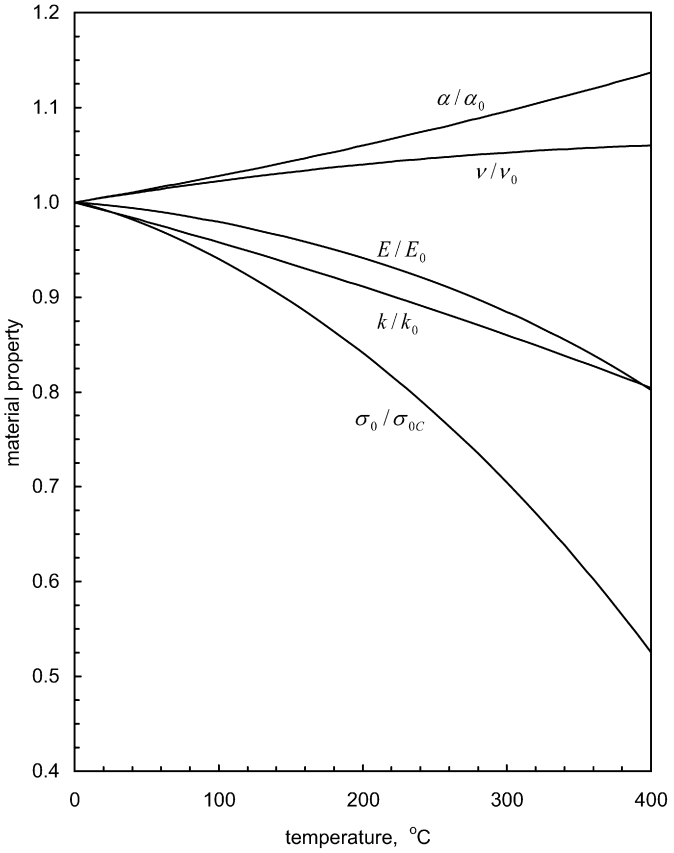

Fig. 1. Variation of physical properties with temperature for high strength low alloy steel.

$$E = E_0\left[1+\frac{T}{E_1\ln(T/E_2)}\right] \tag{4}$$

$$\sigma_0 = \sigma_{0C}\left[1+\frac{T}{\sigma_{01}\ln(T/\sigma_{02})}\right] \tag{5}$$

where $E_0 = 200$ [GPa], $E_1 = 2000$ [°C], $E_2 = 1100$ [°C], $\sigma_{0C} = 410$ [MPa], $\sigma_{01} = 600$ [°C], and $\sigma_{02} = 1630$ [°C]. Fig. 1 shows the variation of dimensionless physical properties with temperature in the range $[0 \leqslant T \leqslant 400\,^{\circ}\mathrm{C}]$. It is seen that, while σ_0, E, and k all decrease with temperature by 48%, 20%, and 20%, in that order, ν and α both increase by 6% and 14%, respectively. The lowest impact is on the Poisson's ratio $\nu(T)$, whereas the highest impact is on the yield limit $\sigma_0(T)$.

In the following sections a computational thermoelastic model is developed to critically evaluate the effect of temperature-dependent material properties in thermomechanical calculations with an emphasis on the Poisson's ratio. The analytical stress and deformation expressions for constant property calculations are also assembled, and, using these expressions, various limits of engineering interest are derived.

2. The thermoelastic model

2.1. Temperature distributions

The temperature distribution $T(r)$ in long cylinders and tubes under uniform energy generation q is governed by the

steady-state heat conduction equation [2]

$$\frac{1}{r}\frac{\mathrm{d}}{\mathrm{d}r}\left[k(T)r\frac{\mathrm{d}T}{\mathrm{d}r}\right]+q=0 \tag{6}$$

with r being the radial coordinate. The solution of Eq. (6) for a cylinder with outer radius b having a constant surface temperature $T(b)=0$ is

$$k_0T+\frac{k_1}{2}T^2+\frac{k_2}{3}T^3=\frac{q}{4}\left(b^2-r^2\right) \tag{7}$$

whereas the solution for a tube of inner radius a having boundary conditions: $-k(\mathrm{d}T/\mathrm{d}r)_{r=a}=0$ and $T(b)=0$ is

$$k_0T+\frac{k_1}{2}T^2+\frac{k_2}{3}T^3=\frac{q}{4}\left[2a^2\ln\left(\frac{r}{b}\right)+b^2-r^2\right] \tag{8}$$

These cubic solutions give three roots at any radial location. However, only one of these roots falls into the calculation domain. It should be noted that the thermoelastic equation, which will be derived next, is not limited to these temperature fields. It is valid for any prescribed temperature distribution.

2.2. The governing equation

The derivation of the thermoelastic equation is performed in terms of formal nondimensional and normalized variables. These are: radial coordinate: $\bar{r}=r/b$, normal stress: $\bar{\sigma}_j=\sigma_j/\sigma_{0C}$, normal strain: $\bar{\varepsilon}_j=\varepsilon_j E_0/\sigma_{0C}$, radial displacement: $\bar{u}=uE_0/(\sigma_{0C}\,b)$, head load: $Q=qE_0\alpha_0b^2/(\sigma_{0C}\,k_0)$, the coefficient of thermal expansion: $\bar{\alpha}=\alpha E_0/\sigma_{0C}$, modulus of elasticity: $\overline{E}=E/E_0$, and the uniaxial yield limit: $\bar{\sigma}_0=\sigma_0/\sigma_{0C}$. The equations given below are written in terms of these variables, but the overbars will be dropped. A state of generalized plane strain and small deformations are assumed. The strain displacement relations for small strains: $\varepsilon_r=u'$, $\varepsilon_\theta=u/r$, the equation of equilibrium in radial direction: $\sigma_\theta=(r\,\sigma_r)'$ and the equations of generalized Hooke's law:

$$\varepsilon_r=\frac{1}{E}\left[\sigma_r-\nu(\sigma_\theta+\sigma_z)\right]+\int_{T_0}^{T}\alpha(T)\,\mathrm{d}T \tag{9}$$

$$\varepsilon_\theta=\frac{1}{E}\left[\sigma_\theta-\nu(\sigma_r+\sigma_z)\right]+\int_{T_0}^{T}\alpha(T)\,\mathrm{d}T \tag{10}$$

$$\varepsilon_z=\frac{1}{E}\left[\sigma_z-\nu(\sigma_r+\sigma_\theta)\right]+\int_{T_0}^{T}\alpha(T)\,\mathrm{d}T \tag{11}$$

form the basis for the formulation [2,6,15]. In the above, a prime indicates differentiation with respect to radial coordinate r, and T_0 stands for a reference temperature. In a state of generalized plane strain $\varepsilon_z=$ constant, and from Eq. (11) the axial stress is determined as

$$\sigma_z=E\varepsilon_z+\nu(\sigma_r+\sigma_\theta)-E\int_{T_0}^{T}\alpha(T)\,\mathrm{d}T \tag{12}$$

Bringing in the stress function $Y(r)$ in terms of radial stress as $Y(r)=r\sigma_r$, one obtains $\sigma_\theta=Y'(r)$ from the equation of equilibrium. Eliminating the axial stress σ_z from Eqs. (9), (10), and using the stress function $Y(r)$, the total strains become

$$\varepsilon_r=\frac{1}{E}\left[\frac{(1-\nu^2)}{r}Y-\nu(1+\nu)Y'\right]+(1+\nu)\int_{T_0}^{T}\alpha(T)\,\mathrm{d}T-\nu\,\varepsilon_z \tag{13}$$

$$\varepsilon_\theta=-\frac{1}{E}\left[\frac{\nu(1+\nu)}{r}Y-\left(1-\nu^2\right)Y'\right]+(1+\nu)\int_{T_0}^{T}\alpha(T)\,\mathrm{d}T-\nu\varepsilon_z \tag{14}$$

The thermoelastic equation is obtained by the substitution of Eqs. (13) and (14) in the compatibility relation $(r\,\varepsilon_\theta)'=\varepsilon_r$. The result is

$$\begin{aligned}&\frac{\mathrm{d}^2Y}{\mathrm{d}r^2}+\left[\frac{1}{r}-\frac{1}{E}\frac{\mathrm{d}E}{\mathrm{d}r}-\frac{2\nu}{1-\nu^2}\frac{\mathrm{d}\nu}{\mathrm{d}r}\right]\frac{\mathrm{d}Y}{\mathrm{d}r}\\&\quad-\left[\frac{1}{r}-\frac{\nu}{E(1-\nu)}\frac{\mathrm{d}E}{\mathrm{d}r}+\frac{1+2\nu}{1-\nu^2}\frac{\mathrm{d}\nu}{\mathrm{d}r}\right]\frac{Y}{r}\\&=\frac{E}{1-\nu^2}\left[\varepsilon_z-\int_{T_0}^{T}\alpha(T)\,\mathrm{d}T\right]\frac{\mathrm{d}\nu}{\mathrm{d}r}\\&\quad-\frac{E}{1-\nu}\frac{\mathrm{d}}{\mathrm{d}r}\int_{T_0}^{T}\alpha(T)\,\mathrm{d}T\end{aligned} \tag{15}$$

A derivative of the form $\mathrm{d}/\mathrm{d}r[\Phi(T)]$ is to be evaluated by the use of the chain rule, i.e.

$$\frac{\mathrm{d}\Phi}{\mathrm{d}r}=\frac{\mathrm{d}\Phi}{\mathrm{d}T}\frac{\mathrm{d}T}{\mathrm{d}r} \tag{16}$$

It is noted that if Poisson's ratio is assumed to be constant, then $\nu'=0$ and $\nu=\nu_0$ and (15) reduces to

$$\begin{aligned}&\frac{\mathrm{d}^2Y}{\mathrm{d}r^2}+\left(\frac{1}{r}-\frac{1}{E}\frac{\mathrm{d}E}{\mathrm{d}r}\right)\frac{\mathrm{d}Y}{\mathrm{d}r}-\left(\frac{1}{r}-\frac{\nu_0}{E(1-\nu_0)}\frac{\mathrm{d}E}{\mathrm{d}r}\right)\frac{Y}{r}\\&\quad=-\frac{E}{1-\nu_0}\frac{\mathrm{d}}{\mathrm{d}r}\int_{T_0}^{T}\alpha(T)\,\mathrm{d}T\end{aligned} \tag{17}$$

which is the thermoelastic equation used in earlier studies (see, for example [4,13]). Furthermore, for temperature-independent material properties $E'=0$, $E=1$ and $\alpha=\alpha_0$, Eq. (17) reduces to the classical plane strain thermoelastic equation of Cauchy–Euler nonhomogeneous type [16,17] given by

$$r^2\frac{\mathrm{d}^2Y}{\mathrm{d}r^2}+r\frac{\mathrm{d}Y}{\mathrm{d}r}-Y=-\frac{\alpha_0}{1-\nu_0}r^2\frac{\mathrm{d}T}{\mathrm{d}r} \tag{18}$$

The solution to the thermoelastic equation (15) provides elastic stresses in plane strain axisymmetric thermal stress problems with temperature-dependent material properties. Although this equation is a linear ODE, the coefficients of Y and Y' are so complicated that its closed form solution could not be found. However, an accurate numerical solution can be obtained by the use of the shooting method as described in [3,11,12].

3. Analytical stresses and limits

These stresses are based on the general solution of Eq. (18). Traction free boundary conditions are used. Elastic limit heat loads are calculated using von Mises' yield criterion. For constant properties (CP) and plane strain this criterion reads [16]

$$\sigma_Y = \sqrt{\frac{1}{2}\left[(\sigma_r-\sigma_\theta)^2+(\sigma_r-\sigma_z)^2+(\sigma_\theta-\sigma_z)^2\right]} \tag{19}$$

Note that the material failure with respect to plastic deformation takes place as soon as $\sigma_Y = 1$.

3.1. Heat generating cylinders

For constant thermal conductivity, i.e. $k = k_0$, and by the use of nondimensional heat generation $Q = qE_0\alpha_0 b^2/(\sigma_{0C}\, k_0)$ Eq. (7) reduces to

$$T(r) = \frac{Q}{4\alpha_0}\left(1-r^2\right) \tag{20}$$

which accompanies the solution of Eq. (18) to estimate the thermoelastic response of cylinders.

3.1.1. Axially constrained ends

The distributions of stress components and radial displacement are

$$\sigma_r = -\frac{Q(1-r^2)}{16(1-\nu_0)}; \qquad \sigma_\theta = -\frac{Q(1-3r^2)}{16(1-\nu_0)}$$
$$\sigma_z = -\frac{Q[2(1-r^2)-\nu_0]}{8(1-\nu_0)} \tag{21}$$

$$u = \frac{Qr(1+\nu_0)(3-2\nu_0-r^2)}{16(1-\nu_0)} \tag{22}$$

The largest differences between the magnitudes of the principal stresses occur at the center; accordingly, the cylinder yields at this location. The elastic limit heat load is determined using von Mises' criterion, Eq. (19), to be

$$Q_{\mathrm{EL}} = \frac{16(1-\nu_0)}{3-2\nu_0} \tag{23}$$

Substitution of Q_{EL} in Eqs. (21), (22) results in maximum distributions of response variables. These are

$$\sigma_{r,\max} = -\frac{1-r^2}{3-2\nu_0}; \qquad \sigma_{\theta,\max} = -\frac{1-3r^2}{3-2\nu_0}$$
$$\sigma_{z,\max} = -\frac{2(2-\nu_0-2r^2)}{3-2\nu_0} \tag{24}$$

$$u_{\max} = \frac{r(1+\nu_0)(3-2\nu_0-r^2)}{3-2\nu_0} \tag{25}$$

Furthermore, for $\nu_0 = 3/10$, the elastic limit heat load is $Q_{\mathrm{EL}} = 14/3$, and the corresponding numerical values of the stresses at the location of yielding, i.e. at the center, turn out to be

$$\sigma_{r,\max}(0) = \sigma_{\theta,\max}(0) = -\frac{5}{12}; \qquad \sigma_{z,\max}(0) = -\frac{17}{12} \tag{26}$$

The maximum stresses and displacement are bounded according to the relations

$$|\sigma_{r,\max}| \leqslant \frac{5}{12}; \qquad \sigma_{\theta,\max} \leqslant \frac{5}{6}; \qquad |\sigma_{z,\max}| \leqslant \frac{17}{12} \tag{27}$$

$$u_{\max} \leqslant \frac{26}{15\sqrt{5}} \tag{28}$$

3.1.2. Axially unconstrained ends

The stresses and radial displacement are

$$\sigma_r = -\frac{Q(1-r^2)}{16(1-\nu_0)}; \qquad \sigma_\theta = -\frac{Q(1-3r^2)}{16(1-\nu_0)}$$
$$\sigma_z = -\frac{Q(1-2r^2)}{8(1-\nu_0)} \tag{29}$$

$$u = \frac{Qr[3-r^2(1+\nu_0)-\nu_0]}{16(1-\nu_0)} \tag{30}$$

From $\int \sigma_z \,\mathrm{d}A = 0$ with $\mathrm{d}A$ belonging to the cross-section, the axial strain is determined to be

$$\varepsilon_z = Q/8 \tag{31}$$

The heat generating cylinder with axially unconstrained ends undergoes plastic deformation at the free surface. The von Mises elastic limit is

$$Q_{\mathrm{EL}} = 8(1-\nu_0) \tag{32}$$

Hence, maximum distributions of the stresses and displacement become

$$\sigma_{r,\max} = -\frac{1}{2}\left(1-r^2\right); \qquad \sigma_{\theta,\max} = -\frac{1}{2}\left(1-3r^2\right)$$
$$\sigma_{z,\max} = -1+2r^2 \tag{33}$$

$$u_{\max} = \frac{1}{2}r\left[3-\nu_0-r^2(1+\nu_0)\right] \tag{34}$$

We also note that

$$\varepsilon_{z,\max} = 1-\nu_0 \tag{35}$$

For $\nu_0 = 3/10$, the values of elastic limit heat load and the axial strain are $Q_{\mathrm{EL}} = 28/5$, and $\varepsilon_{z,\max} = 0.7$, and the corresponding numerical values of the stresses at the location of yielding turn out to be

$$\sigma_{r,\max}(1) = 0, \qquad \sigma_{\theta,\max}(1) = \sigma_{z,\max}(1) = 1 \tag{36}$$

The maximum stresses and displacement are bounded according to the relations

$$|\sigma_{r,\max}| \leqslant \frac{1}{2}; \qquad \sigma_{\theta,\max} \leqslant 1; \qquad |\sigma_{z,\max}| \leqslant 1 \tag{37}$$

$$u_{\max} \leqslant \frac{27}{10\sqrt{13}} \tag{38}$$

3.2. Heat generating tubes

For CP solutions, the temperature distribution given by Eq. (8) takes the form

$$T(r) = \frac{Q}{4\alpha_0}\left(1-r^2+2a^2\ln r\right) \tag{39}$$

3.2.1. Axially constrained ends

The stresses and displacement are

$$\sigma_r = \big(Q\{4a^4(1-r^2)\ln a - (1-a^2)\big[(r^2-a^2)(1-r^2)+4a^2r^2\ln r\big]\}\big) \big/\big(16r^2(1-a^2)(1-\nu_0)\big) \tag{40}$$

$$\sigma_\theta = -\big(Q\{4a^4(1+r^2)\ln a + (1-a^2)\big[r^2(1-3r^2)+a^2(1+5r^2)+4a^2r^2\ln r\big]\}\big) \big/\big(16r^2(1-a^2)(1-\nu_0)\big) \tag{41}$$

$$\sigma_z = -\big(Q\{4a^4\nu_0\ln a + (1-a^2)\big[2(1-r^2)-\nu_0+3a^2\nu_0+4a^2\ln r\big]\}\big) \big/\big(8(1-a^2)(1-\nu_0)\big) \tag{42}$$

$$u = -\frac{Q(1+\nu_0)}{16r(1-a^2)(1-\nu_0)}\{4a^4\big[1+r^2(1-2\nu_0)\big]\ln(a) - (1-a^2)\big[r^2(3-r^2-2\nu_0)-a^2\big[1+r^2(5-6\nu_0)\big] + 4a^2r^2\ln r\big]\} \tag{43}$$

The tube yields at the inner surface, i.e. at $r=a$, and the elastic limit is determined as

$$Q_{\mathrm{EL}} = 8(1-a^2)(1-\nu_0)/\sqrt{D} \tag{44}$$

in which

$$D = (1-a^2)^2\big[3-3\nu_0+\nu_0^2-2a^2(3-7\nu_0+3\nu_0^2) + a^4(7-15\nu_0+9\nu_0^2)\big] + 4a^2(1-a^2)\big[3-\nu_0-2a^2(2-4\nu_0+\nu_0^2) + a^4(1-\nu_0)(5-6\nu_0)\big]\ln a + 16a^4\big[1-a^2(1-\nu_0)+a^4(1-\nu_0)^2\big](\ln a)^2 \tag{45}$$

The limiting distributions of the stresses and displacement then become

$$\sigma_{r,\max} = \big(4a^4(1-r^2)\ln a - (1-a^2)\big[(r^2-a^2)(1-r^2)+4a^2r^2\ln r\big]\big) \big/\big(2r^2\sqrt{D}\big) \tag{46}$$

$$\sigma_{\theta,\max} = -\big(4a^4(1+r^2)\ln a + (1-a^2)\big[r^2(1-3r^2) + a^2(1+5r^2)+4a^2r^2\ln r\big]\big)\big/\big(2r^2\sqrt{D}\big) \tag{47}$$

$$\sigma_{z,\max} = -\big(4a^4\nu_0\ln a + (1-a^2)\big[2-2r^2-\nu_0(1-3a^2) + 4a^2\ln r\big]\big)/\sqrt{D} \tag{48}$$

$$u_{\max} = -\frac{1+\nu_0}{2r\sqrt{D}}\{4a^4\big[1+r^2(1-2\nu_0)\big]\ln a - (1-a^2)\big[r^2(3-2\nu_0-r^2) - a^2\big[1+r^2(5-6\nu_0)\big]+4a^2r^2\ln r\big]\} \tag{49}$$

At the location of onset of yield, the values of the maximum stresses are

Table 1
Elastic limit heat loads and bounds for response variables

a	Q_{EL}	$\lvert\sigma_{r,\max}\rvert \leqslant$	$\sigma_{\theta,\max} \leqslant$	$\lvert\sigma_{z,\max}\rvert \leqslant$	$u_{\max} \leqslant$
0.1	4.03518	0.278363	0.699622	1.15047	0.650417
0.2	4.62576	0.229290	0.735768	1.15253	0.682976
0.3	5.59626	0.187275	0.772351	1.15394	0.715390
0.4	7.15194	0.150644	0.806765	1.15461	0.745398
0.5	9.75948	0.118320	0.838355	1.15465	0.772530

$$\sigma_{r,\max}(a) = 0 \tag{50}$$

$$\sigma_{\theta,\max}(a) = -\frac{1-a^4+4a^2\ln a}{\sqrt{D}} \tag{51}$$

$$\sigma_{z,\max}(a) = -\big((1-a^2)\big[2-\nu_0-a^2(2-3\nu_0)\big] + 4\big[a^2-a^4(1-\nu_0)\big]\ln a\big)/\sqrt{D} \tag{52}$$

For $\nu_0 = 3/10$, elastic limit heat loads and upper bounds for the response variables are determined exactly for different values of a and tabulated in Table 1 to six significant digits.

3.2.2. Axially unconstrained ends

The distributions of stresses and radial displacement are

$$\sigma_r = \big(Q\{4a^4(1-r^2)\ln a - (1-a^2)\big[(r^2-a^2)(1-r^2)+4a^2r^2\ln r\big]\}\big) \big/\big(16r^2(1-a^2)(1-\nu_0)\big) \tag{53}$$

$$\sigma_\theta = -\big(Q\{4a^4(1+r^2)\ln a + (1-a^2)\big[r^2(1-3r^2)+a^2(1+5r^2)+4a^2r^2\ln r\big]\}\big) \big/\big(16r^2(1-a^2)(1-\nu_0)\big) \tag{54}$$

$$\sigma_z = -\frac{Q\{4a^4\ln a+(1-a^2)[1-2r^2+3a^2+4a^2\ln r]\}}{8(1-a^2)(1-\nu_0)} \tag{55}$$

$$u = -\frac{Q}{16r(1-a^2)(1-\nu_0)}\{4a^4\big[1+\nu_0+r^2(1-3\nu_0)\big]\ln a - (1-a^2)\big[r^2\big(3-r^2(1+\nu_0)-\nu_0\big) - a^2\big(1+r^2(5-7\nu_0)+\nu_0\big)+4a^2r^2(1+\nu_0)\ln r\big]\} \tag{56}$$

and the axial strain is

$$\varepsilon_z = \frac{Q}{8}\left[1-3a^2-\frac{4a^4\ln a}{1-a^2}\right] \tag{57}$$

In contrast to tubes with axially constrained ends, tubes with unconstrained ends yield at the outer surface. The elastic limit heat load is determined to be

$$Q_{\mathrm{EL}} = \frac{8(1-a^2)(1-\nu_0)}{1-4a^2+3a^4-4a^4\ln a} \tag{58}$$

The limit Q_{EL} is used to determine limiting distributions. The results are

$$\sigma_{r,\max} = \big(4a^4(1-r^2)\ln a - (1-a^2)\big[(r^2-a^2)(1-r^2)+4a^2r^2\ln r\big]\big) \big/\big(2r^2\big[1-4a^2+a^4(3-4\ln a)\big]\big) \tag{59}$$

$$\sigma_{\theta,\max} = -\big(4a^4(1+r^2)\ln a + (1-a^2)\big[r^2-3r^4+a^2(1+5r^2)+4a^2r^2\ln r\big]\big) \big/\big(2r^2\big[1-4a^2+a^4(3-4\ln a)\big]\big) \tag{60}$$

Table 2
Elastic limit heat loads and bounds for response variables

a	Q_{EL}	$\lvert\sigma_{r,\max}\rvert \leqslant$	$\sigma_{\theta,\max} \leqslant$	$\sigma_{z,\max} \leqslant$	$u_{\max} \leqslant$	$\varepsilon_{z,\max}$
0.1	5.76766	0.397877	1.0	1.0	0.747523	0.7
0.2	6.28698	0.311633	1.0	1.0	0.744026	0.7
0.3	7.24575	0.242474	1.0	1.0	0.739146	0.7
0.4	8.86496	0.186726	1.0	1.0	0.733530	0.7
0.5	11.6412	0.141134	1.0	1.0	0.727621	0.7

$$\sigma_{z,\max} = -\frac{4a^4 \ln a + (1-a^2)[1-2r^2+3a^2+4a^2\ln r]}{1-4a^2+a^4(3-4\ln a)} \tag{61}$$

$$\begin{aligned} u_{\max} = -\frac{1}{F}\big\{&4a^4\big[1+r^2(1-3\nu_0)+\nu_0\big]\ln a \\ &-\big(1-a^2\big)\big[r^2\big(3-r^2(1+\nu_0)-\nu_0\big) \\ &-a^2\big[1+\nu_0+r^2(5-7\nu_0)\big] \\ &+4a^2r^2(1+\nu_0)\ln r\big]\big\} \end{aligned} \tag{62}$$

and

$$\varepsilon_{z,\max} = 1-\nu_0$$

where

$$F = 2r\big[1-4a^2+a^4(3-4\ln a)\big] \tag{63}$$

Furthermore, at the yield location, the maximum stresses are independent of a and take the values

$$\sigma_{r,\max}(1) = 0; \qquad \sigma_{\theta,\max}(1) = \sigma_{z,\max}(1) = 1 \tag{64}$$

For $\nu_0 = 3/10$, elastic limit heat loads and upper bounds for the response variables are determined exactly for different values of a and tabulated in Table 2.

4. Results and discussion

Before the results are presented, a few points need to be explained. The results based on the shooting solution of Eq. (15), which takes into account the temperature dependency of all properties (α, k, E, σ_0, and ν) as described by the relations (1)–(5), are referred to as true (T). On the other hand, the abbreviation VP refers to the results of Eq. (17), which assumes $\nu = \nu_0 =$ constant, and uses relations (2)–(5) to describe the variations of α, k, E, and σ_0 with temperature. We also propose a simplified temperature-dependent model defined by the expressions

$$\nu = \nu_0 = \text{constant} \tag{65}$$

$$k(T) = k_0(1+k_1T) = k_0\big(1-4.509\times10^{-4}T\big) \tag{66}$$

$$\alpha(T) = \alpha_0(1+\alpha_1T) = \alpha_0\big(1+3.053\times10^{-4}T\big) \tag{67}$$

$$E(T) = E_0(1+E_1T) = E_0\big(1-3.197\times10^{-4}T\big) \tag{68}$$

$$\sigma_0(T) = \sigma_{0C}(1+\sigma_{01}T) = \sigma_{0C}\big(1-8.479\times10^{-4}T\big) \tag{69}$$

where, as in Eqs. (2)–(5), $k_0 = 45$ [W/m °C^2], $\alpha_0 = 11.7\times10^{-6}$ [°C^{-1}], $E_0 = 200$ [GPa] and $\sigma_{0C} = 410$ [MPa]. The coefficients in these relations are obtained by least square fits to material property vs. temperature data (Fig. 1) of high strength low alloy steel. This model accompanies the numerical solution of Eq. (17), and the results are cited as PM. Recently, the effect of the temperature dependency of the yield strength σ_0 on thermomechanical predictions has received some attention [18–20]. To be able to comment on this issue, another model, which takes only temperature dependent σ_0 into account, considering other material parameters as constants, is also included. In this model, the yield strength varies with T according to Eq. (5), and the results are referred to as VYL.

In the following calculations $\nu_0 = 0.3$. Moreover, double precision accuracy is used in all numerical computations. First, a verification of the numerical solution procedure is realized. A tube of inner radius $a = 0.2$ with axially unconstrained ends is considered. The analytical elastic limit heat load is given in Table 2 as $Q_{EL} = 6.28698$. Keeping all physical properties constant at their reference values, Eq. (15) is integrated numerically under $Q = 6.28698$ and the distributions of stresses are calculated. Numerical stresses (solid lines) are compared to the analytical ones (dots) with Eqs. (59)–(61) in Fig. 2(a). In this figure, the nondimensional stress variable ϕ_Y is calculated from

$$\phi_Y = \frac{1}{\sigma_0}\sqrt{\frac{1}{2}\big[(\sigma_r-\sigma_\theta)^2+(\sigma_r-\sigma_z)^2+(\sigma_\theta-\sigma_z)^2\big]} \tag{70}$$

Both solutions agree perfectly. In fact, in all calculations, both solutions agree to at least 6 significant digits. The normalized axial strain, for example, is computed as $\varepsilon_z = 0.6999998889$, the analytical value of which is given in Table 2 as 0.7. Note also that, according to von Mises' yield criterion, Eq. (19), $\phi_Y = 1$ at the plastic–elastic border, and $\phi_Y < 1$ in the elastic region. Hence, ϕ_Y turns out to be a useful global variable not only in monitoring the onset of yield, but also in measuring the error in stress calculations. Moreover, it can be used for both variable property and constant property calculations since $\sigma_0 = 1$ for CP. Following the variation of ϕ_Y in Fig. 2(a), we see that the tube yields at the outer surface since $\phi_Y = 1$ at this location. As a second example, we consider a heat generating cylinder with axially constrained ends. The analytical stress expressions at the limit $Q_{EL} = 14/3 = 4.66667$ are those given by Eq. (24). The distributions of analytical stresses (dots) are compared to those calculated numerically (solid lines) with Eq. (15) in Fig. 2(b). Again perfect agreement is obtained. These calculations show that the numerical solution algorithm performs well and the computer program that implements this algorithm functions properly.

Next, elastic limit heat loads for cylinders and tubes of different inner radius are determined by models CP, VP, PM, and VYL and are compared to those of T in Table 3 for axially constrained ends, and to those in Table 4 for unconstrained ends. The symbols (c), (i), and (o) therein mean center, inner surface, and outer surface respectively, and indicate the location of yielding. As seen in Table 3, estimations obtained by variable physical property models are in agreement with CP predictions as far as the yield location is concerned. However, the solutions with temperature-dependent properties predict lower limits. This is in accordance with expectations because the uniaxial yield limit σ_0 decreases rapidly with increasing temperatures as shown in Fig. 1. On the other hand, the predictions of VP and PM are very close to the most reliable estimations by T.

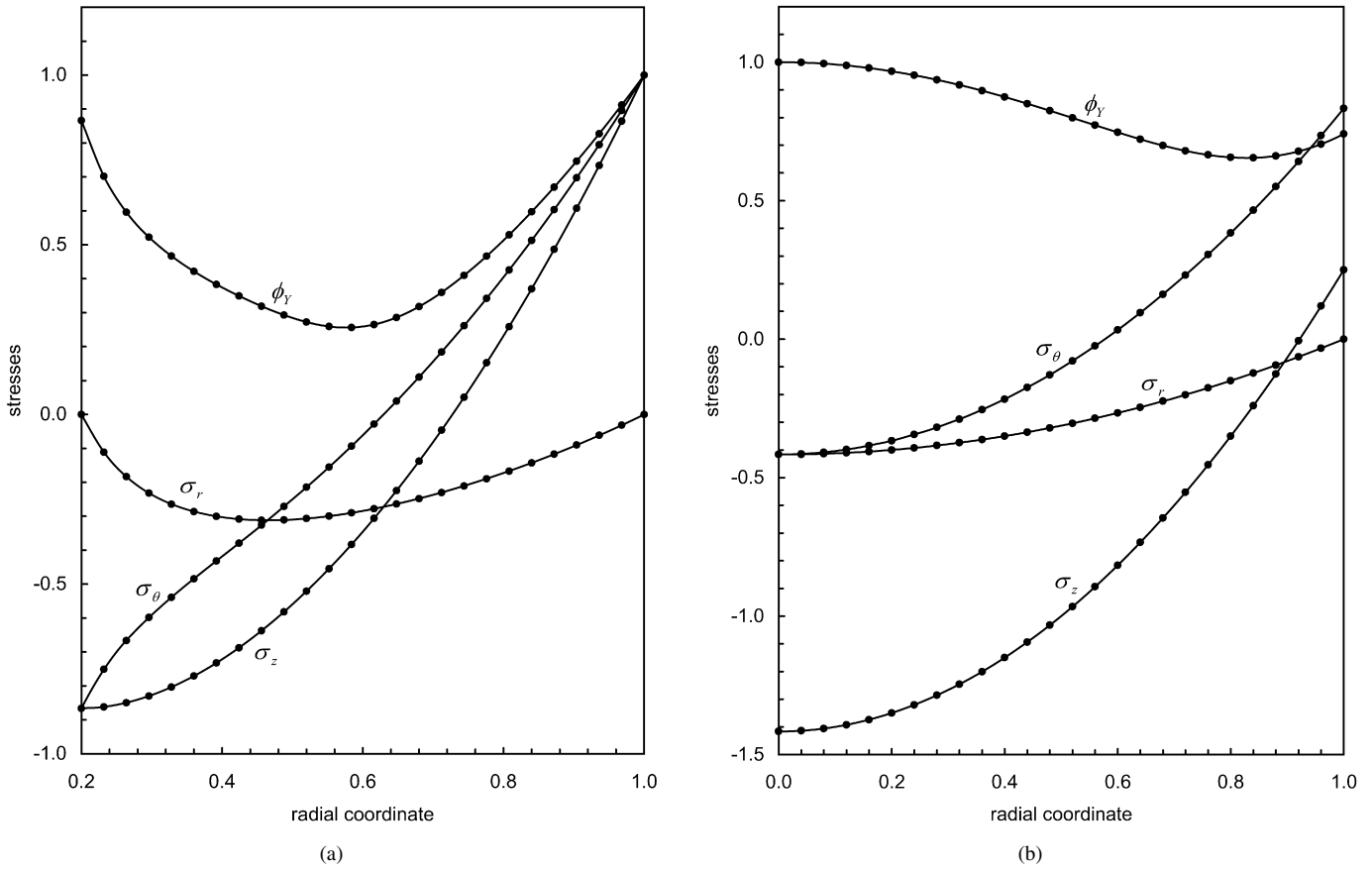

Fig. 2. Comparison of analytical (dots) and numerical (solid lines) stresses keeping physical properties constant for (a) a tube with axially unconstrained ends under the thermal load $Q = 6.28698$, (b) a cylinder with axially constrained ends under the thermal load $Q = 4.66667$.

Table 3
Elastic limit heat loads for axially constrained ends

a	T	CP	VP	PM	VYL
0	3.97477 (c)	4.66667 (c)	3.99945 (c)	3.94846 (c)	4.04554 (c)
0.1	3.50506 (i)	4.03518 (i)	3.52894 (i)	3.46951 (i)	3.61452 (i)
0.2	4.01590 (i)	4.62576 (i)	4.04257 (i)	3.97508 (i)	4.13795 (i)
0.3	4.85614 (i)	5.59626 (i)	4.88743 (i)	4.80657 (i)	4.99963 (i)
0.4	6.20371 (i)	7.15194 (i)	6.24247 (i)	6.13999 (i)	6.38211 (i)
0.5	8.46306 (i)	9.75948 (i)	8.51398 (i)	8.37545 (i)	8.70028 (i)

Table 4
Elastic limit heat loads for unconstrained ends

a	T	CP	VP	PM	VYL
0	5.31723 (o)	5.60000 (o)	5.32571 (o)	5.30460 (o)	5.60000 (o)
0.1	4.74567 (i)	5.76766 (o)	4.78824 (i)	4.75344 (i)	5.06749 (i)
0.2	5.56987 (i)	6.28698 (o)	5.62087 (i)	5.59050 (i)	5.95591 (i)
0.3	6.89237 (o)	7.24575 (o)	6.90417 (o)	6.87711 (o)	7.24575 (o)
0.4	8.43930 (o)	8.86496 (o)	8.45426 (o)	8.42164 (o)	8.86496 (o)
0.5	11.0904 (o)	11.6412 (o)	11.1108 (o)	11.0687 (o)	11.6412 (o)

Relative percent errors calculated via

$$R_{\text{err}} = \left| \frac{\text{T} - \text{Predicted}}{\text{T}} \right| \times 100 \tag{71}$$

in estimating elastic limits for axially constrained ends are calculated with increments of $\Delta a = 0.05$ in the range $[0 \leqslant a \leqslant 0.5]$. The results of these calculations are plotted in Fig. 3. In this figure, dots show the error of CP, squares VP, diamonds PM, and stars VYL. This figure is typical in revealing the necessity of the use of temperature-dependent properties since the error of CP never falls below 15%. The predictions of VYL turn out to be sufficiently accurate since $R_{\text{err}} \ll 5\%$ over the calculation domain. The effect of the use of temperature-dependent ν is not of vital importance in these calculations as the error in VP and PM computations are very close and within 1% throughout.

With reference to Table 4, it is seen again that T, VP, PM and VYL solutions predict lower elastic limits for cylinders and tubes with axially unconstrained ends. What is more, interesting deformation behavior occurs in the case of tubes. Analytical CP solutions indicate that the outer surface is critical and plastic deformation first begins there when Q reaches the limiting values given in Table 4. However, for tubes having nondimensional inner radii 0.1 and 0.2, computations with temperature-dependent properties point to the inner surface as the critical location.

According to T, VP, PM and VYL, for a tube of $a = 0.2$ plastic flow first begins at the inner surface as soon as $Q = Q_{\text{EL}}$, while for the one having $a = 0.3$, it begins at the outer surface. These two different modes of failure with respect to yield imply the existence of a critical inner radius $a = a_{\text{cr}}$ in $0.2 < a_{\text{cr}} < 0.3$ at which plasticization takes place simultaneously at both surfaces. Computations are carried out to determine a_{cr} and the corresponding elastic limit with the use of temperature-

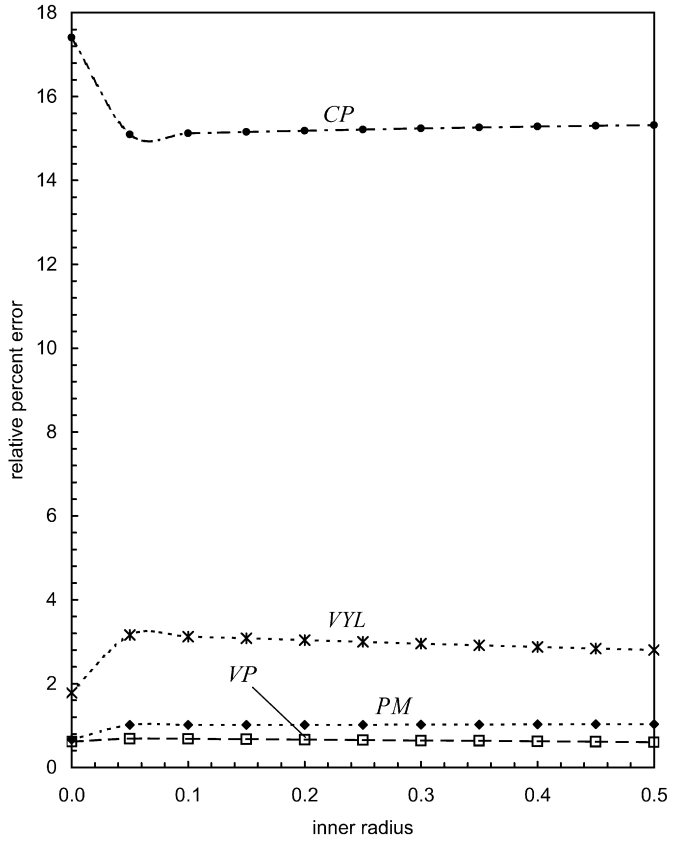

Fig. 3. Relative errors of different models in estimating Q_{EL} for cylinders and tubes with axially constrained ends. Dots belong to CP, squares VP, diamonds PM, and stars VYL.

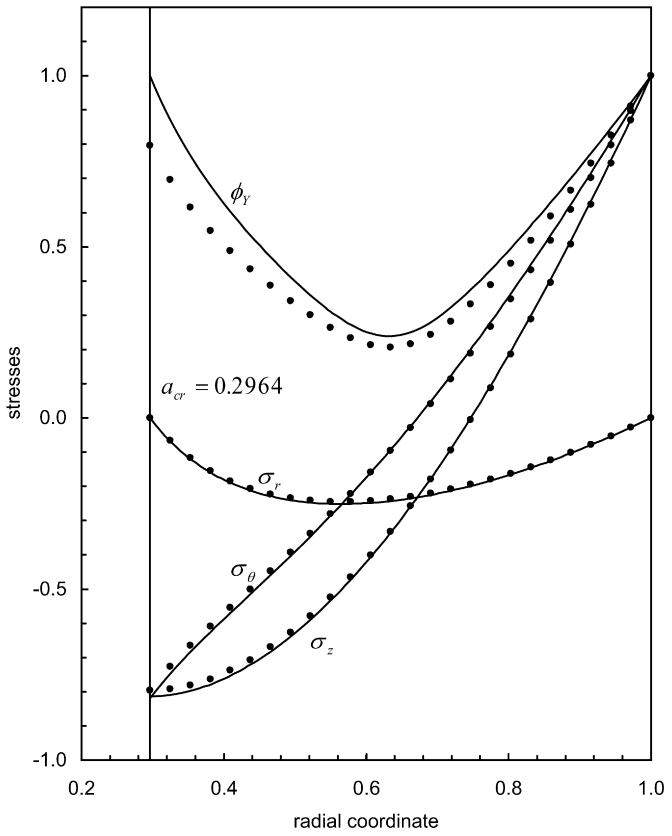

Fig. 4. The elastic response of a tube having inner radius $a = 0.2964$ under $Q = 6.85022$ as predicted by T. Dots belong to CP under $Q = 7.20165$.

dependent models. We find $a_{\mathrm{cr}} = 0.2964$ and $Q_{\mathrm{EL}} = 6.85022$ by T, $a_{\mathrm{cr}} = 0.2857$ and $Q_{\mathrm{EL}} = 6.74078$ by VP, $a_{\mathrm{cr}} = 0.2852$ and $Q_{\mathrm{EL}} = 6.70861$ by PM, and $a_{\mathrm{cr}} = 0.2714$ and $Q_{\mathrm{EL}} = 6.91717$ by VYL. For a tube of inner radius $a = a_{\mathrm{cr}} = 0.2964$, the stresses anticipated by T under the load $Q = Q_{\mathrm{EL}} = 6.85022$ are plotted in Fig. 4 using solid lines. Dots in this figure show analytical stress profiles (CP) for the same tube at its matching analytical limit $Q_{\mathrm{EL}} = 7.20165$. As seen in Fig. 4, the stress state leading to $\phi_Y(a_{\mathrm{cr}}) = \phi_Y(1) = 1$ as predicted by T, is not caught by CP. The errors of CP, VP, PM and VYL in estimating elastic limits for axially unconstrained ends are displayed in Fig. 5. For CP, there appear errors as high as 25% in $0 < a \leqslant 0.3$ since the deformation behavior could not be well predicted by CP in that range. However, CP predictions for $a > 0.3$ are sufficiently accurate. As seen in Fig. 5, errors introduced by VP, and PM are negligible.

The results of normalized axial strain ε_z calculations under $Q = Q_{\mathrm{EL}}$ for cylinders and tubes with axially unconstrained ends are shown in Table 5. The corresponding relative errors can be seen in Fig. 6. Again, large errors appear in case of CP in the problematic range $0 < a \leqslant 0.3$.

Maximum temperatures reached at limit elastic loads and the corresponding percent changes in physical properties, as predicted by T, are tabulated for axially constrained ends in Table 6, and for unconstrained ends in Table 7. The positive and negative values, respectively, indicate percent increase and decrease in the physical properties from $T_0 = 0$ to $T_{\max}$. $T_{\max}$ values for axially unconstrained ends are much larger than those of constrained ends. This may help to explain why CP gives rise to larger errors for smaller values of a in the case of axially unconstrained ends. Among those tubes, the largest $T_{\max}$ corresponds to $a = a_{\mathrm{cr}} = 0.2964$. A tube with $a = a_{\mathrm{cr}}$ can withstand larger temperature gradients.

Table 5
ε_z values of cylinders and tubes

a	T	CP	VP	PM	VYL
0	0.696555	0.7	0.695249	0.695411	0.700000
0.1	0.600133	0.7	0.603844	0.601187	0.615022
0.2	0.647994	0.7	0.652096	0.650773	0.663139
0.3	0.697743	0.7	0.696769	0.696690	0.700000
0.4	0.698216	0.7	0.697405	0.697281	0.700000
0.5	0.698634	0.7	0.697983	0.697842	0.700000

Table 6
Maximum temperatures and changes in material properties for axially constrained ends

a	$T_{\max}$ (°C)	E	σ_0	ν	k	α
0.0	181.11	−5.02	−13.74	3.71	−7.97	5.34
0.1	149.66	−3.75	−10.45	3.18	−6.48	4.32
0.2	151.04	−3.80	−10.58	3.21	−6.55	4.36
0.3	152.38	−3.85	−10.72	3.23	−6.61	4.40
0.4	153.57	−3.90	−10.84	3.25	−6.67	4.44
0.5	154.61	−3.94	−10.94	3.27	−6.72	4.48

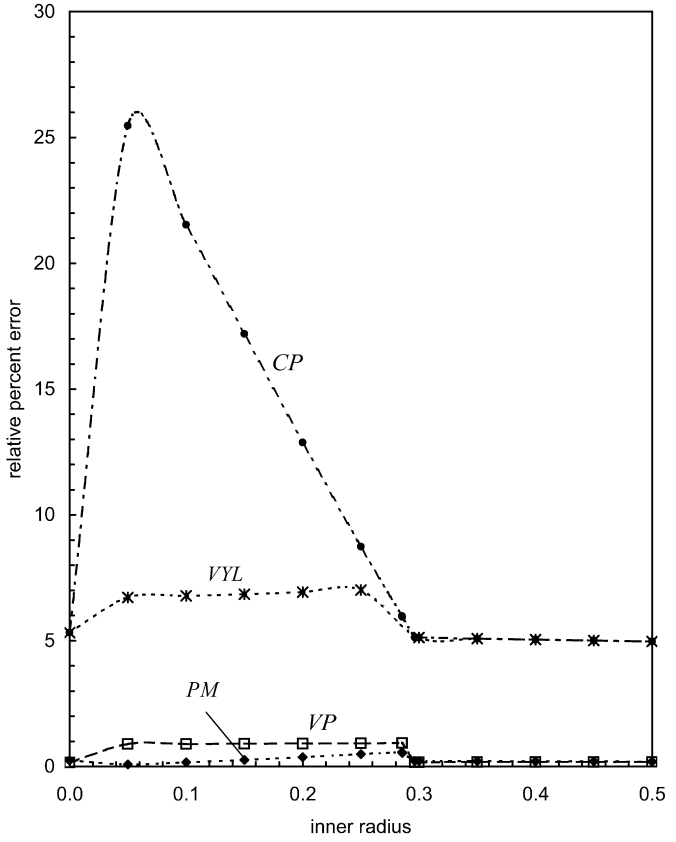

Fig. 5. Relative errors of different models in estimating Q_{EL} for cylinders and tubes with axially unconstrained ends. Dots belong to CP, squares VP, diamonds PM, and stars VYL.

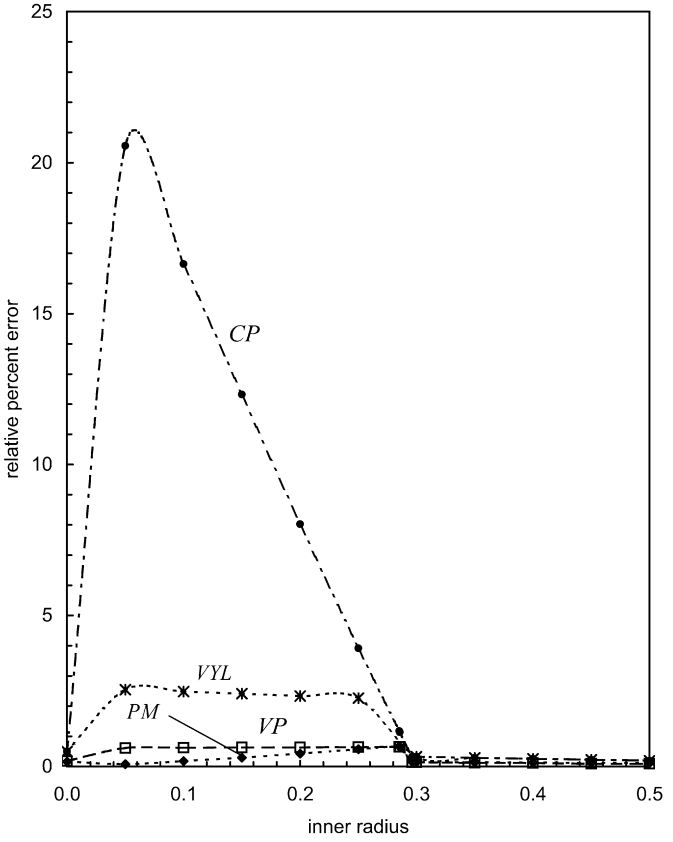

Fig. 6. Relative errors of different models in estimating ε_z for cylinders and tubes. Dots belong to CP, squares VP, diamonds PM, and stars VYL.

Table 7
Maximum temperatures and changes in material properties for unconstrained ends

a	$T_{\max}$ (°C)	E	σ_0	ν	k	α
0.0	246.13	−8.220	−21.70	4.639	−11.19	7.605
0.1	205.29	−6.115	−16.51	4.079	−9.148	6.164
0.2	212.55	−6.465	−17.39	4.184	−9.506	6.415
0.2964	220.06	−6.838	−18.32	4.291	−9.879	6.677
0.3	219.75	−6.822	−18.28	4.286	−9.863	6.666
0.4	211.81	−6.429	−17.30	4.174	−9.469	6.390
0.5	205.03	−6.102	−16.48	4.075	−9.135	6.155

Several examples concerning the elastic states of stress in heat generating cylinders and tubes are given next, comparatively. In the related figures, solid lines will show the true solution (T), dashed lines CP, dots PM and stars VYL. The stress variable ϕ_Y is also plotted in these figures to monitor the error, since the discrepancies in the stress calculations and the effect of $\sigma_0 = \sigma_0(T)$ accumulate in ϕ_Y (see Eq. (70)). Note also that all calculations are performed at the lowest elastic limits predicted by PM. The distributions of stress components and the radial displacement in a cylinder with axially constrained ends predicted by different models at the load $Q = 3.94846$ can be seen in Fig. 7. Fig. 8 displays the stresses and radial displacement in a heat generating cylinder with axially unconstrained ends at $Q = 5.30460$. The deformation behavior of a tube of inner radius $a = 0.5$ with axially constrained ends under the thermal load $Q = 8.37545$ is depicted in Fig. 9. As a final example, the stress response of a tube having inner radius $a = 0.4$ with axially unconstrained ends at $Q = 8.42164$ is displayed in Fig. 10. It is seen in all these figures that the predictions of VYL for the stress and deformation follow CP curves, and that the predictions of PM are in good agreement with those of the true solution.

5. Conclusion

A parametric study is carried out to assess the effect of temperature dependency of the physical properties in calculating the thermomechanical response of heat generating cylinders. The fact that physical properties of engineering materials vary considerably with temperature (see Fig. 1) was the main point motivating this work. Based on the results, several remarks can be made concerning thermally induced deformation of cylinders and tubes.

A thermoelastic calculation using constant physical properties (CP) may lead to errors even in a low temperature range. The errors introduced by CP in predicting critical parameters of engineering interest such as elastic limit heat loads, Q_{EL}, and axial strains, ε_z, can be examined by the help of Figs. 3, 5, and 6. A CP calculation generally results in the overestimation of a parameter. This is because both the modulus of elasticity E, and yield strength σ_0 of the material (steel) decrease sharply with increasing temperatures. As a result, the strength of mate-

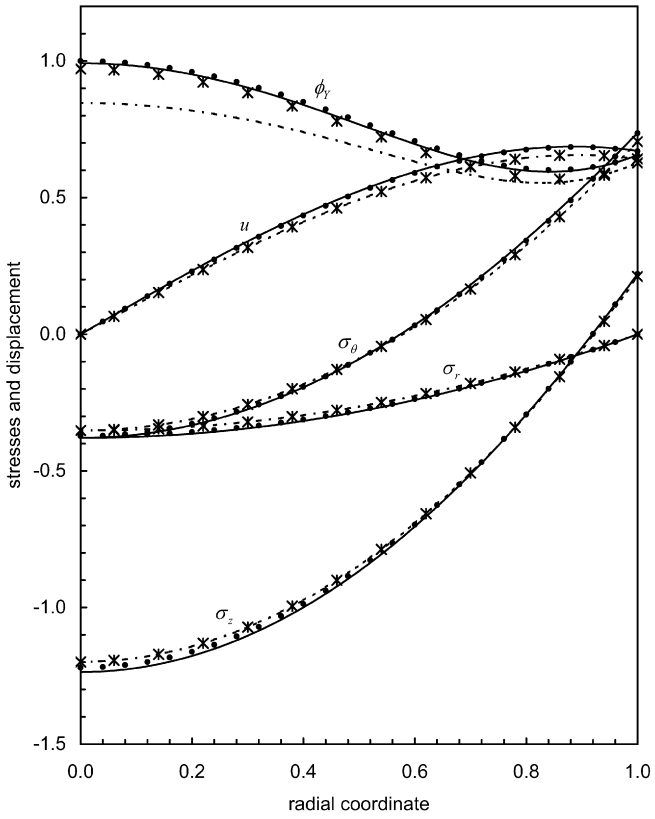

Fig. 7. The elastic response of a cylinder with axially constrained ends under $Q = 3.94846$. Solid lines belong to T, dots PM, stars VYL, and dashed lines CP.

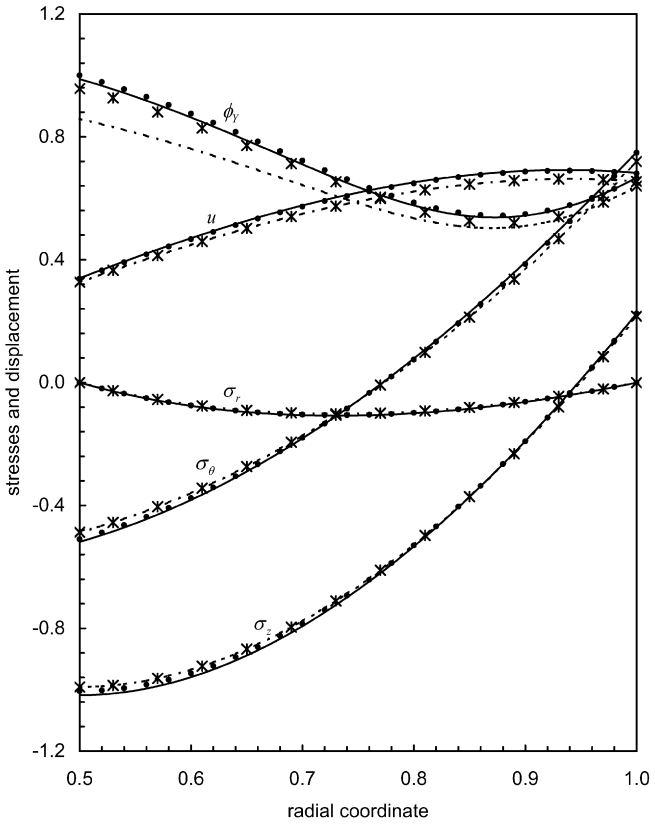

Fig. 9. The elastic response of a tube with axially constrained ends under $Q = 8.37545$. Solid lines belong to T, dots PM, stars VYL, and dashed lines CP.

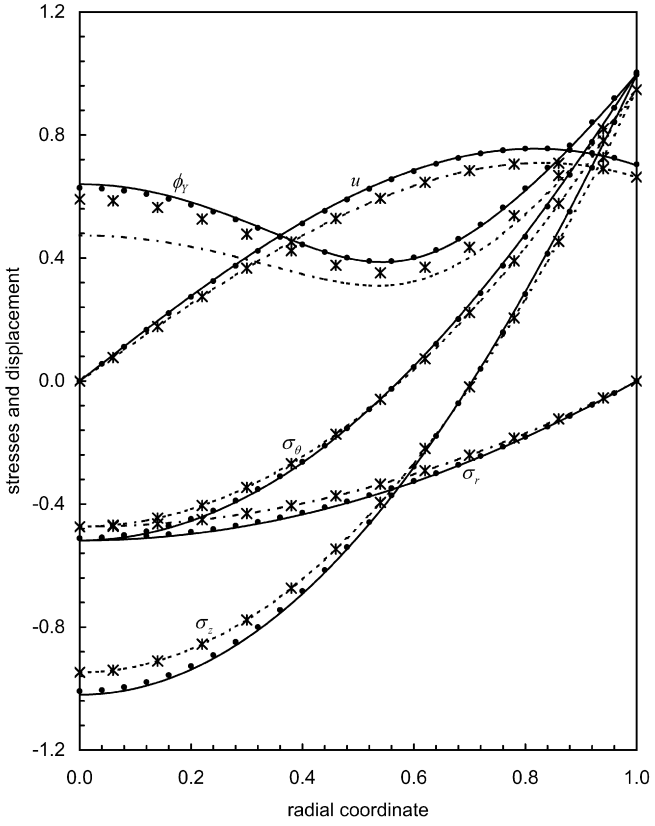

Fig. 8. The elastic response of a cylinder with axially unconstrained ends under $Q = 5.30460$. Solid lines belong to T, dots PM, stars VYL, and dashed lines CP.

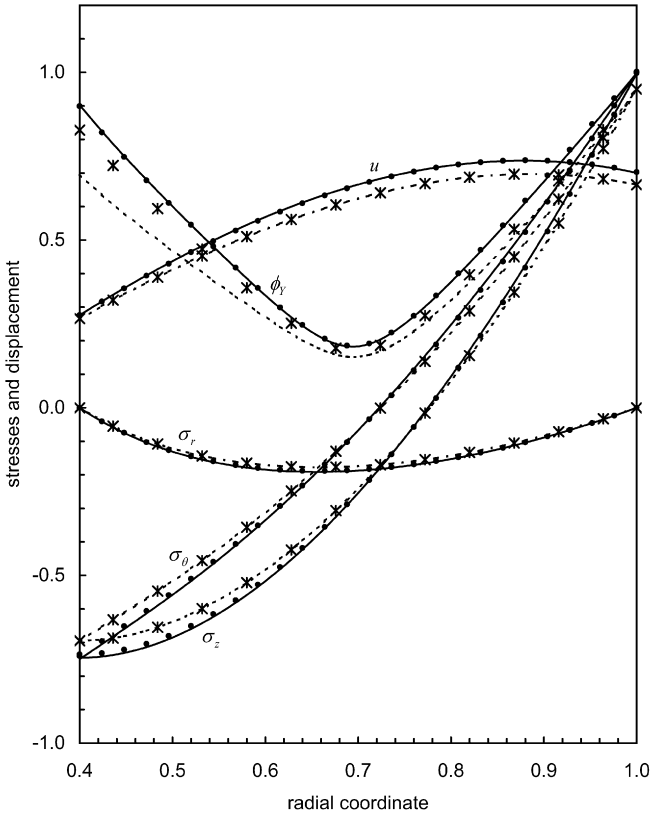

Fig. 10. The elastic response of a tube with axially unconstrained ends under $Q = 8.42164$. Solid lines belong to T, dots PM, stars VYL, and dashed lines CP.

rial to elastically resist thermal loads decreases. This is why the predictions of a model which take only temperature-dependent σ_0 into account turn out to be much better than CP. Figs. 4, 7–10, on the other hand, depict the errors in predicting thermoelastic deformation behavior. Among these, Fig. 4 is typical, in the sense that the actual response of the tube can not be predicted by CP.

The assumption of taking constant Poisson's ratio ν for steel made in the investigations [3,4,8–13] is justified. In fact, an overview of temperature vs. material property data [1] reveals that this assumption is likely to hold for most of the engineering materials. This is pleasing because among the five physical properties, ν is the one for which reliable data is the most difficult to find over a sufficiently wide range of temperatures. In this sense, it also appears that a thermoelastic model that assumes $\nu =$ constant, and includes the linear variation of E, σ_0, α, and k with temperature, serves very well. Such simplified models can easily be constructed for each of the engineering materials under consideration and may accompany intricate multidimensional computations safely and economically.

Acknowledgements

The authors take this opportunity to thank Ms. Yeşim Çöteli and Mr. Robert West in the School of Foreign Languages at METU for carefully editing the revised manuscript.

References

[1] Material Property Database: MPDB Software, JAHM Software, Inc., 29 Valley Rd., North Reading, MA, 01864-1740 (http://www.jahm.com).
[2] B.A. Boley, J.H. Weiner, Theory of Thermal Stresses, Wiley, New York, 1960.
[3] A.N. Eraslan, M.E. Kartal, Stress distributions in cooling fins of variable thickness with and without rotation, Journal of Thermal Stresses 28 (2005) 861–883.
[4] A.N. Eraslan, H. Argeso, Computer solutions of plane strain axisymmetric thermomechanical problems, Turkish Journal of Engineering and Environmental Sciences 29 (2005) 1–13.
[5] H. Ishikawa, Transient thermoelastoplastic stress analysis for a hollow sphere using the incremental theory of plasticity, International Journal of Solids and Structures 13 (1977) 645–655.
[6] N. Noda, Thermal stresses in materials with temperature-dependent properties, in: R.B. Hetnarsky (Ed.), Thermal Stresses I, Elsevier Science, North-Holland, Amsterdam, 1986, pp. 391–483.
[7] N. Noda, Thermal stresses in functionally graded materials, Journal of Thermal Stresses 22 (1999) 477–512.
[8] W. Araki, T. Adachi, A. Yamaji, Thermal stress analysis of thermoviscoelastic hollow cylinder with temperature-dependent thermal properties, Journal of Thermal Stresses 28 (2005) 29–46.
[9] Y. Orcan, A.N. Eraslan, Thermal stresses in elastic–plastic tubes with temperature dependent mechanical and thermal properties, Journal of Thermal Stresses 24 (2001) 1097–1113.
[10] A.N. Eraslan, Y. Orcan, Computation of transient thermal stresses in elastic–plastic tubes: Effect of coupling and temperature dependent physical properties, Journal of Thermal Stresses 25 (2002) 559–572.
[11] A.N. Eraslan, M.E. Kartal, A nonlinear shooting method applied to solid mechanics: Part 1. Numerical solution of a plane stress model, International Journal of Nonlinear Analysis and Phenomena 1 (2004) 27–40.
[12] A.N. Eraslan, H. Argeso, A nonlinear shooting method applied to solid mechanics: Part 2. Numerical solution of a plane strain model, International Journal of Nonlinear Analysis and Phenomena 2 (2005) 31–42.
[13] H. Argeso, A.N. Eraslan, A simple computational model for unified treatment of a class of plane strain thermoplastic stress problems, in: Proceedings of the 6th International Congress on Thermal Stresses, TS2005, vol. 1, 2005, pp. 203–206.
[14] A.N. Eraslan, E. Sener, H. Argeso, Stress distributions in energy generating two-layer tubes subjected to free and radially constrained boundary conditions, International Journal of Mechanical Sciences 45 (2003) 469–496.
[15] S. Timoshenko, J.N. Goodier, Theory of Elasticity, third ed., McGraw–Hill, New York, 1970.
[16] A.N. Eraslan, H. Argeso, On the application of von Mises' yield criterion to a class of plane strain thermal stress problems, Turkish Journal of Engineering and Environmental Sciences 29 (2005) 113–128.
[17] A.C. Uğural, S.K. Fenster, Advanced Strength and Applied Elasticity, third ed., Prentice-Hall, London, 1995.
[18] M. Bengeri, W. Mack, The influence of the temperature dependence of the yield stress on the stress distribution in a thermally assembled elastic–plastic shrink fit, Acta Mechanica 103 (1994) 243–257.
[19] Y. Orcan, M. Gulgec, Influence of the temperature dependence of the yield stress on the stress distribution in a heat-generating tube with free ends, Journal of Thermal Stresses 23 (2000) 529–547.
[20] M. Gulgec, Y. Orcan, Elastic–plastic deformation of a heat generating tube with temperature-dependent yield stress, International Journal of Engineering Science 38 (2000) 89–106.